

SU(3)-flavour breaking in octet baryon masses and axial couplings

Manuel E. Carrillo-Serrano,¹ Ian C. Cloët,² and Anthony W. Thomas¹

¹*CSSM and ARC Centre of Excellence for Particle Physics at the Tera-scale, School of Chemistry and Physics, University of Adelaide, Adelaide SA 5005, Australia*

²*Physics Division, Argonne National Laboratory, Argonne, Illinois 60439, USA*

The lightest baryon octet is studied within a covariant and confining Nambu–Jona-Lasinio model. By solving the relativistic Faddeev equations including scalar and axialvector diquarks, we determine the masses and axial charges for $\Delta S = 0$ transitions. For the latter the degree of violation of SU(3) symmetry arising because of the strange spectator quark(s) is found to be up to 10%.

PACS numbers: 12.38.Aw, 12.39.Ba, 12.39.Fe, 13.30.Ce, 14.20.Jn

Keywords: octet baryon, flavor structure, axial couplings

I. INTRODUCTION

In the quest to fully understand Quantum Chromodynamics (QCD) it is not sufficient to study baryons whose valence quark content consists only of the light u and d quarks. A solid understanding of all members of the baryon octet – that is, the nucleon, Λ , Σ and Ξ multiplets – remains a critical step. Early work on their structure centered on the constituent quark model [1, 2] and the MIT bag model [3], later supplemented by chiral corrections associated with the cloud of virtual pions and kaons that surround a baryon [4–12]. Once their basic properties, such as masses, charge radii, magnetic moments and axial charges had been calculated, attention naturally turned to more complex properties, such as their parton distribution functions [13, 14].

The empirical evidence concerning the structure of the hyperons is naturally far more limited than for nucleons. While we have fairly good data for their masses, magnetic moments and axial charges [15], little or nothing is known concerning their electromagnetic or axial form factors as a function of momentum transfer. Finding ways to explore these properties experimentally would be very valuable. On the other hand, over the last couple of decades lattice QCD has made steady progress in the calculation of octet baryon masses [16–19], including determinations of their isospin mass splittings [20], and certain electroweak matrix elements [21]. These studies have been complemented by a judicious use of chiral effective field theory in order to extrapolate to the physical quark masses. Thus, we now have quite accurate determinations of the hyperon electric [22] and magnetic [23] form factors up to 1.4 GeV², as well as low moments of their parton distribution functions [24]. It has even been possible recently to shed some light on the proton spin puzzle [25, 26] by calculating the spin fractions carried by quarks across the octet [27].

On general grounds one would prefer to have models of octet baryon properties that are covariant as well as respecting the symmetries of QCD. The former is especially important if one wants to investigate parton distributions and form factors at high momentum transfer. The hope in building more sophisticated models is that through comparison with empirical data and lattice QCD studies

one may develop a deeper understanding of how QCD works in the non-perturbative regime, including issues such as the importance and role of diquark correlations and chiral corrections [28], as well as the transition from non-perturbative to perturbative QCD [29].

In this work we investigate the masses and $\Delta S = 0$ axial charges of the octet baryons within the framework of the covariant model of Nambu and Jona-Lasinio (NJL) [30–34], where confinement is simulated by employing proper-time regularization [35–37]. Octet baryons are described by a Poincaré covariant Faddeev equation, where scalar and axialvector diquarks correlations are assumed to play a dominant role. Flavour breaking effects, introduced by a dressed strange quark that is approximately 50% heavier than the dressed light quarks, will also be studied.

The structure of the paper is as follows. Sect. II provides a brief introduction to the NJL model, including a discussion of the Bethe-Salpeter equation for mesons and diquarks. Sect. III introduces the Faddeev equation for octet baryons, discussing the solution for the Poincaré covariant Faddeev amplitude and octet masses. Finally, in Sect. V, the formalism is used to determine the axial charges associated with strangeness conserving beta decays. Sect. VI summarises our findings and presents some concluding remarks.

II. NAMBU–JONA-LASINIO MODEL

The NJL model was formulated as a theory of elementary fermions which encapsulated dynamical chiral symmetry breaking in a transparent manner [30, 31]. With the advent of QCD, it was reformulated with quarks as the fundamental degrees of freedom, such that the symmetries of QCD are respected.¹ In particular the NJL model exhibits dynamical chiral symmetry breaking, which, as implemented in this work, gives rise to approximately 95% of the nucleon mass.

¹ The SU(3) colour gauge symmetry of QCD is a global symmetry of the NJL model.

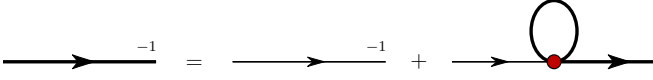


Figure 1. (Colour online) The NJL gap equation in the Hartree-Fock approximation, where the thin line represents the elementary quark propagator, $S_{0q}^{-1}(k) = \not{k} - m_q + i\varepsilon$, and the shaded circle represents the 4-fermion interaction.

The complete three-flavour NJL Lagrangian in the $\bar{q}q$ interaction channel – including only 4-fermion interactions – has the form [34]

$$\begin{aligned} \mathcal{L} = & \bar{\psi} (i\not{\partial} - \hat{m}) \psi \\ & + \frac{1}{2} G_\pi \left[\frac{2}{3} (\bar{\psi}\psi)^2 + (\bar{\psi} \boldsymbol{\lambda} \psi)^2 \right. \\ & \quad \left. - \frac{2}{3} (\bar{\psi} \gamma_5 \psi)^2 - (\bar{\psi} \gamma_5 \boldsymbol{\lambda} \psi)^2 \right] \\ & - \frac{1}{2} G_\rho \left[(\bar{\psi} \boldsymbol{\gamma} \boldsymbol{\lambda} \psi)^2 + (\bar{\psi} \boldsymbol{\gamma} \boldsymbol{\mu} \gamma_5 \boldsymbol{\lambda} \psi)^2 \right] \\ & - \frac{1}{2} G_0 (\bar{\psi} \boldsymbol{\gamma} \boldsymbol{\mu} \psi)^2 - \frac{1}{2} G_5 (\bar{\psi} \boldsymbol{\gamma} \boldsymbol{\mu} \gamma_5 \psi)^2, \end{aligned} \quad (1)$$

where $\boldsymbol{\lambda}$ represents the eight the Gell-Mann matrices and $\hat{m} = \text{diag}[m_u, m_d, m_s]$. The NJL model does not include gluons as explicit degrees of freedom, as such the pointlike quark–quark interaction renders the NJL model non-renormalizable. We regularize the NJL model using the proper-time scheme, which maintains Lorentz and gauge invariance, it also removes unphysical thresholds for the decay of colour singlet bound states in their coloured constituents, thereby simulating quark confinement [35–37].

The dressed quark propagator in the NJL model is obtained from the gap equation illustrated in Fig. 1. The solution for a quark of flavour $q = u, d, s$ has the form

$$S_q(k)^{-1} = \not{k} - M_q + i\varepsilon, \quad (2)$$

where, in the proper-time regularization scheme, the dressed quark masses each satisfy

$$M_q = m_q + \frac{3}{\pi^2} M_q G_\pi \int_{1/\Lambda_{UV}^2}^{1/\Lambda_{IR}^2} d\tau \frac{e^{-\tau M_q^2}}{\tau^2}. \quad (3)$$

In this three-flavour NJL model, defined by Eq. (1), the gap equation does not introduce flavour mixing in the quark propagator, this is in contrast to the two-flavour case which in general has flavour mixing [34].

The quark-quark interaction needed for the two-body interaction kernel in the Faddeev equation (to be described shortly) can be obtained from Eq. (1) using Fierz transformations. Keeping only scalar and axialvector diquark correlations, the NJL interaction Lagrangian in the qq channel reads

$$\begin{aligned} \mathcal{L}_I^{qq} = & G_s \left[\bar{\psi} \gamma_5 C \lambda_a \beta_A \bar{\psi}^T \right] \left[\psi^T C^{-1} \gamma_5 \lambda_a \beta_A \psi \right] \\ & + G_a \left[\bar{\psi} \gamma_\mu C \lambda_s \beta_A \bar{\psi}^T \right] \left[\psi^T C^{-1} \gamma^\mu \lambda_s \beta_A \psi \right], \end{aligned} \quad (4)$$

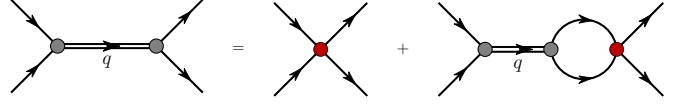


Figure 2. (Colour online) Inhomogeneous Bethe-Salpeter equation for quark–quark (diquark) correlations.

where $C = i\gamma_2\gamma_0$ is the charge conjugation matrix and the couplings G_s and G_a give the strength of the scalar and axialvector qq interactions (with $G_s = -1/3G_\rho + 1/18G_0 + 1/18G_5$ and $G_a = -1/6G_\rho - 1/18G_0 - 1/18G_5$). The flavour matrices are labelled by $\lambda_a = \lambda_2, \lambda_5, \lambda_7$ and $\lambda_s = \lambda_0, \lambda_1, \lambda_3, \lambda_4, \lambda_6, \lambda_8$, where $\lambda_0 \equiv \sqrt{\frac{2}{3}} \mathbb{1}$. Thus, there are three types of scalar and six types of axialvector diquarks. The color $\bar{3}$ matrices are given by $\beta_A = \sqrt{\frac{3}{2}} \lambda_A$ ($A = 2, 5, 7$) [38–40] and hence the interaction terms in Eq. (4) are totally antisymmetric, as demanded by the Pauli principle.

Quark-antiquark and quark-quark bound states are obtained by solving the appropriate Bethe-Salpeter equation, which is illustrated in Fig. 2 for diquarks. The reduced t -matrices for scalar and axial-vector diquarks, with quark flavour content q_1 and q_2 , take the form²

$$\tau_{[q_1 q_2]}(q) = \frac{-4i G_s}{1 + 2 G_s \Pi_{[q_1 q_2]}(q^2)}, \quad (5)$$

$$\begin{aligned} \tau_{\{q_1 q_2\}}^{\mu\nu}(q) = & \frac{-4i G_a}{1 + 2 G_a \Pi_{\{q_1 q_2\}}(q^2)} \\ & \times \left[g^{\mu\nu} + 2 G_a \Pi_{\{q_1 q_2\}}(q^2) \frac{q^\mu q^\nu}{q^2} \right]. \end{aligned} \quad (6)$$

The bubble diagrams are given by

$$\begin{aligned} \Pi_{[q_1 q_2]}(q^2) = & 6i \int \frac{d^4 k}{(2\pi)^4} \text{Tr} [\gamma_5 S_{q_1}(k) \gamma_5 S_{q_2}(k+q)], \end{aligned} \quad (7)$$

$$\begin{aligned} \Pi_{\{q_1 q_2\}}(q^2) \left(g^{\mu\nu} - \frac{q^\mu q^\nu}{q^2} \right) = & 6i \int \frac{d^4 k}{(2\pi)^4} \text{Tr} [\gamma^\mu S_{q_1}(k) \gamma^\nu S_{q_2}(k+q)], \end{aligned} \quad (8)$$

where the flavour and colour traces have been taken, and the remaining trace is over Dirac indices only. The masses of the various diquarks are given by the poles in the corresponding t -matrix, e.g., the scalar diquarks masses are given by the pole condition

$$1 + 2 G_s \Pi_{[q_1 q_2]}(q^2 = M_{[q_1 q_2]}^2) = 0. \quad (9)$$

² Throughout this paper $[q_1 q_2]$ will indicate a quantity associated with a scalar diquark and $\{q_1 q_2\}$ will indicate an object associated with an axialvector diquark quantity.

For the octet baryon calculations we approximate the full diquark t -matrix by a *contact + pole* form, that is

$$\tau_{[q_1 q_2]}(q) \rightarrow 4i G_s - \frac{i Z_{[q_1 q_2]}}{q^2 - M_{[q_1 q_2]}^2 + i\varepsilon}, \quad (10)$$

$$\tau_{\{q_1 q_2\}}^{\mu\nu}(q) \rightarrow 4i G_a - \frac{i Z_{\{q_1 q_2\}}}{q^2 - M_{\{q_1 q_2\}}^2 + i\varepsilon} \left(g^{\mu\nu} - \frac{q^\mu q^\nu}{M_{\{q_1 q_2\}}^2} \right), \quad (11)$$

where the pole residues are given by

$$Z_{[q_1 q_2]}^{-1} = -\frac{1}{2} \frac{\partial}{\partial q^2} \Pi_{[q_1 q_2]}(q^2) \Big|_{q^2=M_{[q_1 q_2]}^2}, \quad (12)$$

$$Z_{\{q_1 q_2\}}^{-1} = -\frac{1}{2} \frac{\partial}{\partial q^2} \Pi_{\{q_1 q_2\}}(q^2) \Big|_{q^2=M_{\{q_1 q_2\}}^2}. \quad (13)$$

III. FADDEEV EQUATIONS FOR OCTET BARYONS

Octet baryons are constructed as solutions to a Poincaré covariant Faddeev equation, which is illustrated in Fig. 3, where the quark–diquark approximation used here has been made explicit [41]. A tractable solution to the Faddeev equation is obtained by employing the static approximation [42] to the quark exchange kernel, where the exchanged quark propagator becomes $S_q(k) \rightarrow -\frac{1}{M_q}$. This approximation has been shown to yield excellent results for nucleon form factors [28] and quark distributions [43–46]. The Faddeev equation for each octet baryon then takes the form

$$\Gamma_B(p, s) = Z_B \Pi_B(p) \Gamma_B(p, s), \quad (14)$$

where B labels an octet baryon, Z_B the corresponding quark exchange kernel and $\Pi_B(p)$ is a diagonal matrix containing the various combinations of quark and diquark propagator. Eq. (14) must be supplemented by a normalization condition, such that the normalized Faddeev vertex reads

$$\Gamma_B(p, s) = \sqrt{-Z_B} \Gamma_{0B}(p, s), \quad (15)$$

where $\Gamma_{0B}(p, s)$ is the unnormalized vertex and the normalization condition that determines Z_B will be discussed shortly.

For equal light quark masses the nucleon, Σ and Ξ Faddeev vertex functions contain one scalar diquark and two types of axial-vector diquark³, with a Dirac structure

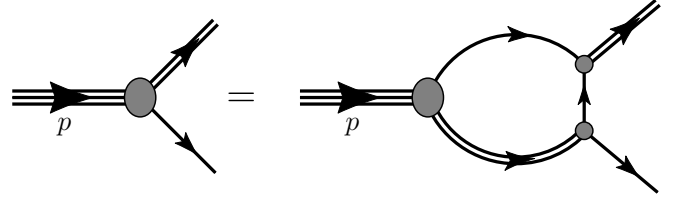


Figure 3. Homogeneous Poincaré covariant Faddeev equation whose solution gives the mass and vertex function for each member of the baryon octet.

of the form

$$\Gamma_b(p, s) = \begin{bmatrix} \Gamma_{q_1[q_1 q_2]}(p, s) \\ \Gamma_{q_1\{q_1 q_2\}}^\mu(p, s) \\ \Gamma_{q_2\{q_1 q_1\}}^\mu(p, s) \end{bmatrix}, \quad (16)$$

$$= \sqrt{-Z_b} \begin{bmatrix} \alpha_1 \\ \alpha_2 \frac{p^\mu}{M_b} \gamma_5 + \alpha_3 \gamma^\mu \gamma_5 \\ \alpha_4 \frac{p^\mu}{M_b} \gamma_5 + \alpha_5 \gamma^\mu \gamma_5 \end{bmatrix} u_b(p, s), \quad (17)$$

where $b = [\text{nucleon}, \Sigma, \Xi]$ and Z_b is the vertex normalization. The Faddeev vertex function for the Λ baryon, with equal u and d quark masses, contains two types of scalar diquark and an axial-vector diquark and therefore reads

$$\Gamma_\Lambda(p, s) = \sqrt{-Z_\Lambda} \begin{bmatrix} \alpha_1 \\ \alpha_2 \\ \alpha_3 \frac{p^\mu}{M_\Lambda} \gamma_5 + \alpha_4 \gamma^\mu \gamma_5 \end{bmatrix} u_\Lambda(p, s). \quad (18)$$

The quark exchange kernel for the nucleon, Σ and Ξ reads

$$Z_b = 3 \begin{bmatrix} \frac{1}{M_1} & \frac{1}{M_1} \gamma_\sigma \gamma_5 & -\frac{\sqrt{2}}{M_2} \gamma_\sigma \gamma_5 \\ \frac{1}{M_1} \gamma_5 \gamma_\mu & \frac{1}{M_1} \gamma_\sigma \gamma_\mu & \frac{\sqrt{2}}{M_2} \gamma_\sigma \gamma_\mu \\ -\frac{\sqrt{2}}{M_2} \gamma_5 \gamma_\mu & \frac{\sqrt{2}}{M_2} \gamma_\sigma \gamma_\mu & 0 \end{bmatrix} \quad (19)$$

where, in each case, M_1 is the mass of the singly represented dressed quark and M_2 the mass of the doubly represented dressed quark.⁴ The factor of 3 is obtained from projecting the kernel onto colour singlet states. For the Λ the quark exchange kernel is given by

$$Z_\Lambda = \begin{bmatrix} 0 & \frac{\sqrt{2}}{M_\ell} & -\frac{\sqrt{2}}{M_\ell} \\ \frac{\sqrt{2}}{M_\ell} & -\frac{1}{M_s} & -\frac{1}{M_s} \gamma_\sigma \gamma_5 \\ -\frac{\sqrt{2}}{M_\ell} \gamma_5 \gamma_\mu & -\frac{1}{M_s} \gamma_5 \gamma_\mu & -\frac{1}{M_s} \gamma_\sigma \gamma_\mu \end{bmatrix}, \quad (20)$$

where M_ℓ is the mass of the dressed light quark. The quark–diquark bubble diagram matrix for the nucleon, Σ

³ For the nucleon, in the $M_u = M_d$ limit, the singly and doubly represented axialvector diquarks are mass degenerate and could therefore be treated as a single type of diquark. However, for the nucleon we will keep the description more general so that the analogy with the other members of the octet is straightforward.

⁴ For the Σ^0 , the term “doubly represented” means the two light quarks of different flavours.

Λ_{IR}	Λ_{UV}	M_ℓ	M_s	G_π	G_ρ	G_s	G_a
0.240	0.645	0.40	0.59	19.0	10.8	7.6	2.6

Table I. Model parameters are constrained to reproduce the physical pion and ρ meson masses; the pion decay constant; the nucleon and Ξ masses and the nucleon axial coupling. The infrared regulator and the dressed u and d quark masses – labelled by M_ℓ – are assigned their values *a priori*. The regularization parameters and dressed quark mass are in units of GeV, while the couplings are in units of GeV^{-2} .

and Ξ reads

$$\Pi_b(p) = \begin{bmatrix} \Pi_{q_2[q_1 q_2]}(p) & 0 & 0 \\ 0 & \Pi_{q_2\{q_1 q_2\}}^{\sigma\nu}(p) & 0 \\ 0 & 0 & \Pi_{q_1\{q_2 q_2\}}^{\sigma\nu}(p) \end{bmatrix}, \quad (21)$$

where for each baryon q_1 is the singly represented dressed quark and q_2 the doubly represented dressed quark. For the Λ the analogous quantity reads

$$\Pi_\Lambda(p) = \begin{bmatrix} \Pi_{s[\ell\ell]}(p) & 0 & 0 \\ 0 & \Pi_{\ell[\ell s]}(p) & 0 \\ 0 & 0 & \Pi_{\ell\{\ell s\}}^{\sigma\nu}(p) \end{bmatrix}. \quad (22)$$

The quark–diquark bubble diagrams are given by

$$\Pi_{q_i[q_j q_k]}(p) = \int \frac{d^4 k}{(2\pi)^4} S_{q_i}(k) \tau_{[q_j q_k]}(p-k), \quad (23)$$

$$\Pi_{q_i\{q_j q_k\}}^{\mu\nu}(p) = \int \frac{d^4 k}{(2\pi)^4} S_{q_i}(k) \tau_{\{q_j q_k\}}^{\mu\nu}(p-k). \quad (24)$$

Finally, the vertex normalization is given by

$$\mathcal{Z}_B^{-1} = \bar{\Gamma}_{0B} \frac{\partial \Pi_B(p)}{\partial p^2} \Gamma_{0B} \Big|_{p^2=M_B^2}. \quad (25)$$

Note, the value of p^2 which satisfies the Faddeev equation for each octet baryon defines its mass, M_B^2 , and at that point the coefficients α_i then define the octet baryon vertex function.

IV. RESULTS FOR OCTET BARYONS MASSES

The NJL model employed in this work has the following parameters: two regularization parameters Λ_{IR} and Λ_{UV} ;

M_K	$M_{[\ell\ell]}$	$M_{[\ell s]}$	$M_{\{\ell\ell\}}$	$M_{\{\ell s\}}$	$M_{\{ss\}}$
0.47	0.68	0.85	1.04	1.17	1.30

Table II. Results for the kaon mass, together with the various diquark masses, where the subscript $\ell = u, d$. Recall that the square brackets label scalar diquarks and the curly brackets axialvector diquarks. All masses are in units of GeV.

Z_π	Z_K	$Z_{[\ell\ell]}$	$Z_{[\ell s]}$	$Z_{\{\ell\ell\}}$	$Z_{\{\ell s\}}$	$Z_{\{ss\}}$
17.8	29.6	14.8	16.4	3.56	3.93	4.29

Table III. Results for the pole residues in the various meson and diquark t -matrices (c.f. Eqs. (10) and (11)).

the dressed quark masses M_u, M_d and M_s ; ⁵ two coupling constants, G_π and G_ρ , from the $\bar{q}q$ NJL Lagrangian, given in Eq. (1); and the two coupling constants G_s and G_a from the qq NJL Lagrangian. The infrared cutoff implements confinement and therefore should be of the order of Λ_{QCD} and we choose $\Lambda_{IR} = 0.240 \text{ GeV}$; for the light-quark dressed masses we choose $M_u = M_d = 0.4 \text{ GeV}$; the ultraviolet cutoff Λ_{UV} and the couplings G_π and G_ρ are constrained by the empirical values for the pion decay constant, the pion mass and the ρ mass; the qq couplings are chosen to reproduce the physical nucleon mass and the nucleon axial coupling constant. Finally, the dressed s -quark mass is fixed to reproduce the empirical mass of the cascade baryon (Ξ). The resulting parameters are summarized in Tab. I.

Results for the kaon mass together with the various diquark masses are given in Tab. II. The splitting between the various scalar diquarks and between the axialvector diquarks is the result of explicit $SU(3)_F$ breaking effects from the strange quark. The empirical light to strange current quark mass ratio in the $\overline{\text{MS}}$ regularization scheme is $m_s/m_q = 27.5 \pm 1.0$ [15], while we find $m_s/m_q = 21.7$. For the analogous dressed quark mass ratio we obtain $M_s/M_q \simeq 1.5$, which illustrates that effects from DCSB are very much suppressed for the heavier strange quark. For completeness we give in Tab. III the pole residues for the meson and diquark t -matrices.

The octet baryon masses obtained by solving the appropriate Faddeev equation, as discussed in Sect. III, are given in Tab. IV. In the $SU(3)_F$ limit all octet baryon masses are degenerate and hence the mass splitting between octet baryons results solely from the heavier s quark

	M_N	M_Λ	M_Σ	M_Ξ
NJL	0.940	1.120	1.234	1.318
Experiment	0.940	1.116	1.193	1.318

Table IV. Results for octet baryon masses and the average experimental mass for the corresponding multiplet. All experimental masses have an error of at most 0.015% but usually it is much less [15]. Because we have $M_u = M_d$ the masses of each member of the various isospin multiplets are degenerate. Recall that the nucleon and Ξ masses were used to determine two of our NJL model parameters. All masses are in GeV.

⁵ Alternatively, one may use the current quark masses m_u, m_d, m_s from the NJL Lagrangian, as the gap equation provides a one-to-one correspondence with the dressed masses.

	α_1	α_2	α_3	α_4	α_5
nucleon	0.418	0.013	-0.259	-0.018	0.366
Λ	0.364	0.278	-0.016	0.440	-
Σ	0.351	0.032	-0.215	-0.021	0.406
Ξ	0.388	0.017	-0.273	-0.015	0.364

Table V. Numerical coefficients that define the Faddeev vertex functions for each member of the baryon octet. The nucleon, Σ and Ξ vertex functions have the form given in Eq. (17) and the Λ vertex function is given in Eq. (18).

mass. The mass splitting between the Λ and Σ baryons is a consequence of the different diquark correlations which dominate their wavefunctions. The Λ baryon contains two types of scalar diquark and one type of axialvector diquark – $[\ell\ell]$, $[ls]$ and $\{\ell s\}$ – while the Σ baryon contains one type of scalar diquark and two types of axialvector diquark – $[ls]$, $\{\ell s\}$ and $\{\ell\ell\}$. Scalar diquarks are more bound than axialvector diquarks – because of their strong connection with the pion and DCSB – and consequently we find that the Λ is approximately 110 MeV lighter than the Σ baryon. This is in reasonable agreement with the empirical mass splitting of approximately 80 MeV. A more precise fit would also need to include chiral corrections. The parameters defining the Faddeev vertex function for each member of the baryon octet are summarized in Tab. V.

V. AXIAL CHARGES

The axial charges of the baryons are important because they connect the strong and weak interactions. They are also related to the quark spin content of the baryons [47]. In fact, assuming $SU(3)$ -flavour symmetry, all octet baryon decays can be parametrized by just three quantities: the Cabbibo angle, θ_C , and the F and D couplings [48, 49].

The axial current of an octet baryon has the form

$$\begin{aligned}
J_{5,\lambda}^{\mu,a}(p', p) &= \langle p', \lambda' | \bar{\psi}_q \gamma^\mu \gamma_5 \lambda_a \psi_q | p, \lambda \rangle, \\
&= \bar{u}(p', \lambda') \left[\gamma^\mu \gamma_5 G_A(Q^2) \right. \\
&\quad \left. + \frac{q^\mu \gamma_5}{2 M_B} G_P(Q^2) + \frac{i \sigma^{\mu\nu} q_\nu \gamma_5}{2 M_B} G_T(Q^2) \right] \lambda_a u(p, \lambda). \quad (26)
\end{aligned}$$

where $q = p' - p$ is the 4-momentum transfer, $Q^2 \equiv -q^2$ and λ, λ' represent the initial and final nucleon helicity, respectively. The scalar functions $G_A(Q^2)$, $G_P(Q^2)$ and $G_T(Q^2)$ label the axial, induced pseudoscalar and induced pseudotensor form factors, respectively. In this work we restrict ourselves to the $q \rightarrow 0$ limit, where the current becomes

$$J_{5,\lambda}^{\mu,a}(p, p) = G_A(0) \bar{u}(p, \lambda) \gamma^\mu \gamma_5 \lambda_a u(p, \lambda). \quad (27)$$

The flavour-triplet axial charge of an octet baryon, g_A^B ,

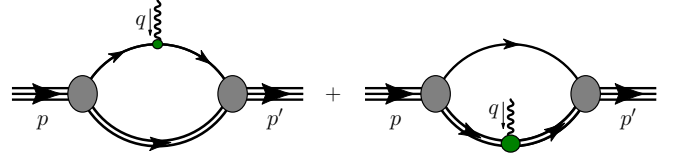


Figure 4. (Colour online) Feynman diagrams representing the axial current for the octet baryons. The diagram on the left is called the quark diagram and the one on the right the diquark diagram. In the diquark diagram the photon interacts with each quark inside the non-pointlike diquark.

is given by the matrix element

$$g_A^B s^\mu = \langle B | \bar{\psi} \gamma^\mu \gamma_5 \lambda_3 \psi | B \rangle = (\Delta u_B - \Delta d_B) s^\mu, \quad (28)$$

where $s^\mu = \bar{u}(p, \lambda) \gamma^\mu \gamma_5 u(p, \lambda)$ is the spin-vector of the octet baryon. The quark-spin fractions of the baryon are defined by

$$\Delta q_B s^\mu = \langle B | \bar{\psi} \gamma^\mu \gamma_5 \hat{P}_q \psi | B \rangle, \quad (29)$$

where the u and d quark projection operators are given by

$$\hat{P}_q = \frac{1}{2} \left(\frac{2}{3} \mathbb{1} \pm \lambda_3 + \frac{1}{\sqrt{3}} \lambda_8 \right), \quad (30)$$

and the plus sign corresponds to the u quark.

The various spin-fractions for the octet baryons under consideration are given by the sum of the six Feynman diagrams represented in Fig. 4 and have the structure

$$\begin{aligned}
\Delta u_p &= f_{u\{ud\}}^Q + f_{u\{ud\}}^Q \\
&\quad + 2 f_{u\{ud\}}^D + 2 f_{u\{ud\}}^D + 4 f_{d\{uu\}}^D + 2 f_{u\{ud\} \leftrightarrow u\{ud\}}^D, \quad (31)
\end{aligned}$$

$$\begin{aligned}
\Delta d_p &= f_{d\{uu\}}^Q + 2 f_{u\{ud\}}^D + 2 f_{u\{ud\}}^D - 2 f_{u\{ud\} \leftrightarrow u\{ud\}}^D, \quad (32)
\end{aligned}$$

$$\Delta u_{\Sigma^-} = 0, \quad (33)$$

$$\begin{aligned}
\Delta d_{\Sigma^-} &= f_{d\{ds\}}^Q + f_{d\{ds\}}^Q \\
&\quad + 2 f_{d\{ds\}}^D + 2 f_{d\{ds\}}^D + 4 f_{s\{dd\}}^D + 2 f_{d\{ds\} \leftrightarrow d\{ds\}}^D, \quad (34)
\end{aligned}$$

$$\Delta u_{\Xi^-} = 0, \quad (35)$$

$$\begin{aligned}
\Delta d_{\Xi^-} &= f_{d\{ss\}}^Q + 2 f_{s\{ds\}}^D + 2 f_{s\{ds\}}^D - 2 f_{s\{ds\} \leftrightarrow s\{ds\}}^D. \quad (36)
\end{aligned}$$

The nomenclature for these Feynman diagrams is: a superscript Q implies that the operator acts directly on a quark (*quark diagram*) and a superscript D implies that the operator acts on (a quark inside) a diquark (*diquark diagram*); the notation $q_1 [q_2 q_3]$ indicates a diagram with quark content $q_1 q_2 q_3$ contains only a scalar diquark of quark content $q_2 q_3$. Similarly the notation $q_1 \{q_2 q_3\}$ indicates a diagram contains only an axialvector diquark of quark content $q_2 q_3$; and finally the notation $q_1 \{q_2 q_3\} \leftrightarrow q_1 [q_2 q_3]$ indicates the sum of the two diagrams where the operator induces a transition between scalar

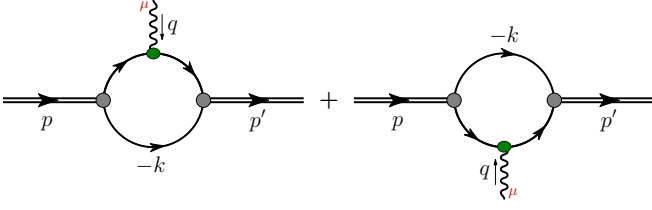


Figure 5. (Colour online) Feynman diagrams that represent the diquark axial current. The shaded circles are the diquark Bethe-Salpeter vertices and the shaded oval is the $\gamma^\mu \gamma_5$ vertex.

and axialvector diquarks of flavour $q_2 q_3$. The numerical coefficients arise from the flavour structure of the operator and the Faddeev amplitude.

In general the quark diagram with a scalar diquark spectator reads

$$f_{q_1[q_2 q_3]}^Q \bar{u} \gamma^\mu \gamma_5 u = \bar{\Gamma}_{q_1[q_2 q_3]}(p) \int \frac{d^4 k}{(2\pi)^4} \times S_{q_1}(k) \gamma^\mu \gamma_5 S_{q_1}(k) \tau_{[q_2 q_3]}(p+k) \Gamma_{q_1[q_2 q_3]}(p), \quad (37)$$

and the analogous diagram with an axialvector diquark spectator is given by

$$f_{q_1\{q_2 q_3\}}^Q \bar{u} \gamma^\mu \gamma_5 u = \bar{\Gamma}_{q_1\{q_2 q_3\},\alpha}(p) \int \frac{d^4 k}{(2\pi)^4} \times S_{q_1}(k) \gamma^\mu \gamma_5 S_{q_1}(k) \tau_{\{q_2 q_3\}}^{\alpha\beta}(p+k) \Gamma_{q_1\{q_2 q_3\},\beta}(p). \quad (38)$$

Similarly, the general form of the diquark diagram with a scalar diquark reads

$$f_{q_1[q_2 q_3]}^D \bar{u} \gamma^\mu \gamma_5 u = \bar{\Gamma}_{q_1[q_2 q_3]}(p) \int \frac{d^4 k}{(2\pi)^4} i S_{q_1}(p+k) \times \tau_{[q_2 q_3]}(k) \Lambda_{[q_2 q_3]}^\mu \tau_{[q_2 q_3]}(k) \Gamma_{q_1[q_2 q_3]}(p), \quad (39)$$

and the analogous diagram with an axialvector diquark is given by

$$f_{q_1\{q_2 q_3\}}^D \bar{u} \gamma^\mu \gamma_5 u = \bar{\Gamma}_{q_1\{q_2 q_3\},\alpha}(p) \int \frac{d^4 k}{(2\pi)^4} i S_{q_1}(p+k) \times \tau_{\{q_2 q_3\}}^{\alpha\sigma}(k) \Lambda_{\sigma\eta,\{q_2 q_3\}}^\mu \tau_{\{q_2 q_3\}}^{\eta\beta}(k) \Gamma_{q_1\{q_2 q_3\},\nu}(p), \quad (40)$$

where $\Lambda_{[q_2 q_3]}^\mu$ and $\Lambda_{\alpha\beta,\{q_2 q_3\}}^\mu$ represent, respectively, the interaction of a scalar and axialvector diquark, with an axialvector current, in the $q \rightarrow 0$ and on-shell limits. Because the scalar diquark has spin-zero, we have $\Lambda_{[q_2 q_3]}^\mu = 0$, while for the axialvector diquark we have

$$\Lambda_{\{q_2 q_3\}}^{\mu,\alpha\beta}(p) = 3i \int \frac{d^4 k}{(2\pi)^4} \times \text{Tr}_D [\gamma^\beta S(p+k) \gamma^\mu \gamma_5 S(p+k) \gamma^\alpha S(k)], \quad (41)$$

$$= g_A^{\{q_2 q_3\}} i \varepsilon^{\mu\alpha\beta\lambda} p_\lambda, \quad (42)$$

where α is the initial and β the final diquark polarization. The Feynman diagram for this contribution is illustrated

Δu_n	Δd_n	Δu_{Σ^-}	Δd_{Σ^-}	Δu_{Ξ^-}	Δd_{Ξ^-}
1.145	0.331	0	-1.048	0	0.313

Table VI. Results for the spin fractions in the nucleon, Σ , and Ξ .

in Fig. 5. For the various axialvector diquarks we find: $g_A^{\{\ell\ell\}} = -0.216$, $g_A^{\{\ell s\}} = -0.194$, $g_A^{\{\ell s\}} = -0.213$ and $g_A^{\{ss\}} = -0.194$ ⁶. Note that in evaluating Eq. (41) we have used the on-shell condition, $\varepsilon_\alpha(p) p^\alpha = 0$, for both the initial and final axialvector diquark.

The final Feynman diagram represents the mixing between the scalar and axialvector diquarks induced by the axial current, this diagram reads

$$f_{q_1[q_2 q_3] \leftrightarrow q_1\{q_2 q_3\}}^D \equiv f_{q_1[q_2 q_3] \rightarrow q_1\{q_2 q_3\}}^D + f_{q_1\{q_2 q_3\} \rightarrow q_1[q_2 q_3]}^D, \quad (43)$$

where each contribution is given by⁷

$$f_{q_1[q_2 q_3] \rightarrow q_1\{q_2 q_3\}}^D \bar{u} \gamma^\mu \gamma_5 u = \bar{\Gamma}_{q_1\{q_2 q_3\},\alpha}(p) i \int \frac{d^4 k}{(2\pi)^4} S_{q_1}(p+k) \tau_{\{q_2 q_3\}}^{\alpha\sigma}(k) \Lambda_{\sigma,[q_2 q_3] \rightarrow \{q_2 q_3\}}^\mu \tau_{[q_2 q_3]}(k) \Gamma_{q_1[q_2 q_3]}(p), \quad (44)$$

$$f_{q_1\{q_2 q_3\} \rightarrow q_1[q_2 q_3]}^D \bar{u} \gamma^\mu \gamma_5 u = \bar{\Gamma}_{q_1[q_2 q_3]}(p) i \int \frac{d^4 k}{(2\pi)^4} S_{q_1}(p+k) \tau_{[q_2 q_3]}(k) \Lambda_{\sigma,\{q_2 q_3\} \rightarrow [q_2 q_3]}^\mu \tau_{\{q_2 q_3\}}^{\sigma\alpha}(k) \Gamma_{q_1\{q_2 q_3\},\alpha}(p). \quad (45)$$

The diquark transition vertices are given by

$$\Lambda_{[q_2 q_3] \rightarrow \{q_2 q_3\}}^{\mu\alpha} = 3i \int \frac{d^4 k}{(2\pi)^4} \times \text{Tr}_D [\gamma_5 S(p+k) \gamma^\mu \gamma_5 S(p+k) \gamma^\alpha S(k)], \quad (46)$$

$$\Lambda_{\{q_2 q_3\} \rightarrow [q_2 q_3]}^{\mu\alpha} = 3i \int \frac{d^4 k}{(2\pi)^4} \times \text{Tr}_D [\gamma^\alpha S(p+k) \gamma^\mu \gamma_5 S(p+k) \gamma_5 S(k)]. \quad (47)$$

These vertices have the general form

$$\Lambda_{[q_2 q_3] \rightarrow \{q_2 q_3\}}^{\mu\alpha} = a_{q_2 q_3} g^{\mu\alpha} + b_{q_2 q_3} p^\mu p^\alpha = -\Lambda_{\{q_2 q_3\} \rightarrow [q_2 q_3]}^{\mu\alpha}. \quad (48)$$

For the various diquark transitions we find: $a_{\ell\ell} = -0.054$, $a_{\ell s} = -0.052$, $a_{\ell s} = -0.048$, $b_{\ell\ell} = 0.092$, $b_{\ell s} = 0.096$ and $b_{\ell s} = 0.115$.

⁶ In our notation the underlined character denotes the quark that interacts with the photon. For example in $\{\ell s\}$ the light quark interacts with the photon in the axialvector diquark.

⁷ Note, when calculating these diagrams we in practice consider a small momentum transfer so that we can correctly identify p'^2 and p^2 with the initial and final diquark mass squared.

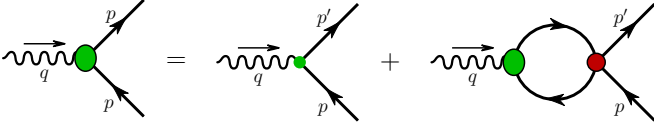


Figure 6. (Colour online) Inhomogeneous Bethe-Salpeter equation whose solution gives the quark-axialvector vertex, represented as the large shaded oval. The small dot is the inhomogeneous driving term, while the shaded circle is the $\bar{q}q$ interaction kernel. Only the ρ interaction channel contributes.

Evaluating these diagrams gives the spin-fractions which we summarize in Tab. VI. In addition to these body form factor contributions, the axial charge of the quark receives a finite renormalization. This renormalization is given by the inhomogeneous BSE illustrated in Fig. 6. The renormalized axial charge of the light quark is given by

$$g_A^q = \frac{1}{1 + 2 G_{a_1} \Pi_{AA}^{(T)}(0)}, \quad (49)$$

where $\Pi_{AA}^{(T)}(q^2)$ is the transverse piece of the bubble diagram

$$\begin{aligned} \Pi_{AA}^{\mu\nu}(q^2) &= 6i \int \frac{d^4k}{(2\pi)^4} \text{Tr}_D [\gamma^\mu \gamma_5 S(k+q) \gamma^\nu \gamma_5 S(k)], \\ &\equiv \left(g^{\mu\nu} - \frac{q^\mu q^\nu}{q^2} \right) \Pi_{AA}^{(T)}(q^2) + \frac{q^\mu q^\nu}{q^2} \Pi_{AA}^{(L)}(q^2). \end{aligned} \quad (50)$$

The coupling G_{a_1} is adjusted ($G_{a_1} = 1.0$) to give $M_{a_1} = 1.26$ GeV. The unrenormalized quark axial charge is unity, however for the renormalized axial charge we find $g_A^q = 0.935$. The value of the axial charge for octet baryon strangeness conserving transitions, for the bare case (“Bare”) and for the case with a renormalized axial quark vertex (“BSE”) are given in Tab. VII.

The axial charges for the octet baryons also receive corrections from the meson cloud. In order to preserve the correct non-analytic behavior, required by chiral symmetry, it is necessary to compute these at the hadronic level [50, 51]. This requires the meson-baryon coupling constants and form factors. The former are given by the appropriate Goldberger-Treiman relation, which is respected because the NJL model respects chiral symmetry. The latter are related to the hadron sizes. Since both the axial charges and hadron sizes in the present model are very close to those calculated in the cloudy bag model (CBM) [4, 52], we can take the meson corrections directly from the work of Kubodera et al. [53]. In practice this means that our results should be multiplied by 0.92 for g_A^Σ , 0.90 for g_A^Ξ and 0.95 for g_A^Ξ . Our final results, including corrections from the quark vertex renormalization and the meson cloud are shown in Tab. VII. The only experimental value we have available is g_A^n . The values of the vector form factors $f_1(0)$ are 1, $\sqrt{2}$ and 1 for the nucleon, Σ , and Ξ , respectively. This comes from charge

	Bare	BSE	BSE + CBM	exp’t/Ref. [55]
$(g_A/f_1)^n$	1.48	1.38	1.27	1.2701 ± 0.0025
$(g_A/f_1)^\Sigma$	0.52	0.49	0.44	0.44
$(g_A/f_1)^\Xi$	-0.31	-0.29	-0.28	-0.32

Table VII. Axial charges for the different beta decays with $\Delta S = 0$ in three cases: Bare, treats the quark as a point-like particle, without structure and without a meson cloud; BSE, includes the renormalization of the quark axial charge through the solution of the BSE and, finally, including the BSE renormalization as well as meson cloud corrections computed within the CBM. As the experimental result is only known for the nucleon case, for the Σ and Ξ we show the results from the CBM computation in Ref. [55], modified very slightly to reproduce the current experimental value of g_A^n .

conservation when the electromagnetic form factors are computed in the octet.

We are now in a position to determine the size of SU(3)-flavour breaking effects for the axial charges of the octet baryons, using the SU(3)-flavour parametrization of Ref. [48], namely

$$n \rightarrow p + \nu_e + e^- \implies (g_A/f_1)^n = F + D, \quad (51)$$

$$\Sigma^- \rightarrow \Sigma^0 + \nu_e + e^- \implies (g_A/f_1)^\Sigma = F, \quad (52)$$

$$\Xi^- \rightarrow \Xi^0 + \nu_e + e^- \implies (g_A/f_1)^\Xi = F - D. \quad (53)$$

Within our model the values of F and D may be computed by choosing any pair of the previous relations. We call $F_{\Sigma(\Xi)}$ and $D_{\Sigma(\Xi)}$ the parameters calculated from $(g_A/f_1)^{\Sigma(\Xi)}$ and $(g_A/f_1)^n$. From Tab. VII we obtain

$$\begin{aligned} F_\Sigma &= (g_A/f_1)^\Sigma = 0.441, \\ D_\Sigma &= (g_A/f_1)^n - (g_A/f_1)^\Sigma = 0.829, \end{aligned} \quad (54)$$

and

$$\begin{aligned} F_\Xi &= \frac{1}{2}((g_A/f_1)^n + (g_A/f_1)^\Xi) = 0.496, \\ D_\Xi &= \frac{1}{2}((g_A/f_1)^n - (g_A/f_1)^\Xi) = 0.774. \end{aligned} \quad (55)$$

The discrepancies suggest SU(3)-flavour symmetry breaking effects of around 10%, with $F_\Sigma/F_\Xi = 0.89$ and $D_\Sigma/D_\Xi = 1.07$. Since the strangeness conserving β -decays for the Σ^- and Ξ^- have not yet been measured, this result should be viewed as a prediction to be tested experimentally. We note that even larger SU(3) violation has been reported in the context of the proton spin problem [54].

In addition, a comparison of our results with the cloudy bag model computations performed in Ref. [55] shows that g_A^Σ is the same in both models, whereas g_A^Ξ is slightly smaller in magnitude in our work. The calculation of Ref. [55] includes one-gluon exchange and center of mass corrections, plus recoil effects and a rescaling factor to reproduce the experimental g_A^n .

The other source of “data” with which our model might be compared are lattice QCD calculations. There has

recently been good progress in the calculation of the electromagnetic form factors for the octet baryons [22, 23], using chiral extrapolations of the lattice results. Clearly an extension of that work to weak form factors would provide a valuable test our model predictions.

VI. CONCLUSIONS

We have computed the masses and the $\Delta S = 0$ axial charges of the baryon octet using a confining NJL model. The model results for the masses are in good agreement with the experimental values. While there are currently no measurements of the $\Delta S = 0$ axial charges, other than for the neutron, we did find very close agreement between our results and those found within the cloudy bag model. Since there is currently considerable discussion concerning the degree of violation of SU(3) symmetry, the deviation of order 10% which we found is significant.

It will be important to extend the present investigation to calculate the chiral corrections explicitly within this model. Given the new lattice results for octet baryon electromagnetic form factors, we look forward to simulations of a similar quality for the axial form factors. Meantime, it would be very interesting to extend the present model to calculate the hyperon electromagnetic form factors.

ACKNOWLEDGEMENTS

ICC thanks Wolfgang Bentz invaluable conversations. This material is based upon work supported by the U.S. Department of Energy, Office of Science, Office of Nuclear Physics, under contract number DE-AC02-06CH11357; and the Australian Research Council through the ARC Centre of Excellence in Particle Physics at the Terascale and an ARC Australian Laureate Fellowship FL0992247 (AWT).

-
- [1] A. Le Yaouanc, L. Oliver, O. Pene and J. -C. Raynal, Phys. Rev. D **18**, 1591 (1978).
 - [2] N. Isgur and G. Karl, Phys. Rev. D **20**, 1191 (1979).
 - [3] A. Chodos, R. L. Jaffe, K. Johnson and C. B. Thorn, Phys. Rev. D **10**, 2599 (1974).
 - [4] S. Theberge, A. W. Thomas and G. A. Miller, Phys. Rev. D **22**, 2838 (1980) [Erratum-ibid. D **23**, 2106 (1981)].
 - [5] S. Theberge and A. W. Thomas, Phys. Rev. D **25**, 284 (1982).
 - [6] F. Myhrer, G. E. Brown and Z. Xu, Nucl. Phys. A **362**, 317 (1981).
 - [7] F. Myhrer and Z. Xu, Phys. Lett. B **108**, 372 (1982).
 - [8] K. Tsushima, T. Yamaguchi, Y. Kohyama and K. Kubodera, Nucl. Phys. A **489**, 557 (1988).
 - [9] H. Weigel, R. Alkofer and H. Reinhardt, Nucl. Phys. A **576**, 477 (1994) [hep-ph/9310309].
 - [10] G. Wagner, A. J. Buchmann and A. Faessler, Phys. Rev. C **58**, 3666 (1998) [nucl-th/9809015].
 - [11] D. Diakonov, In *Peniscola 1997, Advanced school on non-perturbative quantum field physics* 1-55 [hep-ph/9802298].
 - [12] I. C. Cloët, D. B. Leinweber and A. W. Thomas, Phys. Rev. C **65**, 062201 (2002) [hep-ph/0203023].
 - [13] C. Boros and A. W. Thomas, Phys. Rev. D **60**, 074017 (1999) [hep-ph/9902372].
 - [14] D. Diakonov, V. Petrov, P. Pobylitsa, M. V. Polyakov and C. Weiss, Nucl. Phys. B **480**, 341 (1996) [hep-ph/9606314].
 - [15] J. Beringer *et al.* [Particle Data Group Collaboration], Phys. Rev. D **86**, 010001 (2012).
 - [16] S. Durr, Z. Fodor, J. Frison, C. Hoelbling, R. Hoffmann, S. D. Katz, S. Krieg and T. Kurth *et al.*, Science **322**, 1224 (2008) [arXiv:0906.3599 [hep-lat]].
 - [17] R. D. Young and A. W. Thomas, Phys. Rev. D **81**, 014503 (2010) [arXiv:0901.3310 [hep-lat]].
 - [18] A. Walker-Loud, H. -W. Lin, D. G. Richards, R. G. Edwards, M. Engelhardt, G. T. Fleming, P. Hagler and B. Musch *et al.*, Phys. Rev. D **79**, 054502 (2009) [arXiv:0806.4549 [hep-lat]].
 - [19] S. Aoki *et al.* [PACS-CS Collaboration], Phys. Rev. D **79**, 034503 (2009) [arXiv:0807.1661 [hep-lat]].
 - [20] S. Borsanyi, S. Durr, Z. Fodor, C. Hoelbling, S. D. Katz, S. Krieg, L. Lellouch and T. Lippert *et al.*, arXiv:1406.4088 [hep-lat].
 - [21] H. -W. Lin and K. Orginos, Phys. Rev. D **79**, 034507 (2009) [arXiv:0712.1214 [hep-lat]].
 - [22] P. E. Shanahan, A. W. Thomas, R. D. Young, J. M. Zanotti, R. Horsley, Y. Nakamura, D. Pleiter and P. E. L. Rakow *et al.*, arXiv:1403.1965 [hep-lat].
 - [23] P. E. Shanahan, A. W. Thomas, R. D. Young, J. M. Zanotti, R. Horsley, Y. Nakamura, D. Pleiter and P. E. L. Rakow *et al.*, Phys. Rev. D **89**, 074511 (2014) [arXiv:1401.5862 [hep-lat]].
 - [24] I. C. Cloët, R. Horsley, J. T. Londergan, Y. Nakamura, D. Pleiter, P. E. L. Rakow, G. Schierholz and H. Stuben *et al.*, Phys. Lett. B **714**, 97 (2012) [arXiv:1204.3492 [hep-lat]].
 - [25] J. Ashman *et al.* [European Muon Collaboration], Phys. Lett. B **206**, 364 (1988).
 - [26] F. Myhrer and A. W. Thomas, Phys. Lett. B **663**, 302 (2008) [arXiv:0709.4067 [hep-ph]].
 - [27] P. E. Shanahan, A. W. Thomas, K. Tsushima, R. D. Young and F. Myhrer, Phys. Rev. Lett. **110**, no. 20, 202001 (2013) [arXiv:1302.6300 [nucl-th]].
 - [28] I. C. Cloët, W. Bentz and A. W. Thomas, arXiv:1405.5542 [nucl-th].
 - [29] I. C. Cloët, C. D. Roberts and A. W. Thomas, Phys. Rev. Lett. **111**, 101803 (2013) [arXiv:1304.0855 [nucl-th]].
 - [30] Y. Nambu and G. Jona-Lasinio, Phys. Rev. **122**, 345 (1961).
 - [31] Y. Nambu and G. Jona-Lasinio, Phys. Rev. **124**, 246 (1961).
 - [32] U. Vogl and W. Weise, Prog. Part. Nucl. Phys. **27**, 195 (1991).
 - [33] T. Hatsuda and T. Kunihiro, Phys. Rept. **247**, 221 (1994) [hep-ph/9401310].
 - [34] S. P. Klevansky, Rev. Mod. Phys. **64**, 649 (1992).

- [35] D. Ebert, T. Feldmann and H. Reinhardt, Phys. Lett. B **388**, 154 (1996) [hep-ph/9608223].
- [36] G. Hellstern, R. Alkofer and H. Reinhardt, Nucl. Phys. A **625**, 697 (1997) [hep-ph/9706551].
- [37] W. Bentz and A. W. Thomas, Nucl. Phys. A **696**, 138 (2001) [nucl-th/0105022].
- [38] N. Ishii, W. Bentz and K. Yazaki, Nucl. Phys. A **587**, 617 (1995).
- [39] N. Ishii, W. Bentz and K. Yazaki, Phys. Lett. B **301**, 165 (1993).
- [40] N. Ishii, W. Bentz and K. Yazaki, Phys. Lett. B **318**, 26 (1993).
- [41] I. R. Afnan and A. W. Thomas, Top. Curr. Phys. **2**, 1 (1977).
- [42] A. Buck, R. Alkofer and H. Reinhardt, Phys. Lett. B **286**, 29 (1992).
- [43] I. C. Cloët, W. Bentz and A. W. Thomas, Phys. Lett. B **621**, 246 (2005) [hep-ph/0504229].
- [44] I. C. Cloët, W. Bentz and A. W. Thomas, Phys. Rev. Lett. **95**, 052302 (2005) [nucl-th/0504019].
- [45] I. C. Cloët, W. Bentz and A. W. Thomas, Phys. Lett. B **659**, 214 (2008) [arXiv:0708.3246 [hep-ph]].
- [46] W. Bentz, I. C. Cloët, T. Ito, A. W. Thomas and K. Yazaki, Prog. Part. Nucl. Phys. **61**, 238 (2008) [arXiv:0711.0392 [nucl-th]].
- [47] R. L. Jaffe and A. Manohar, Nucl. Phys. B **337**, 509 (1990).
- [48] J. M. Gaillard and G. Sauvage, Ann. Rev. Nucl. Part. Sci. **34**, 351 (1984).
- [49] H. Hogaasen and F. Myhrer, Z. Phys. C **68**, 625 (1995) [hep-ph/9501414].
- [50] A. W. Thomas and G. Krein, Phys. Lett. B **456**, 5 (1999) [nucl-th/9902013].
- [51] A. W. Thomas and G. Krein, Phys. Lett. B **481**, 21 (2000) [nucl-th/0004008].
- [52] A. W. Thomas, Adv. Nucl. Phys. **13**, 1 (1984).
- [53] K. Kubodera, Y. Kohyama, K. Oikawa and C. W. Kim, Nucl. Phys. A **439**, 695 (1985).
- [54] S. D. Bass and A. W. Thomas, Phys. Lett. B **684**, 216 (2010) [arXiv:0912.1765 [hep-ph]].
- [55] T. Yamaguchi, K. Tsushima, Y. Kohyama and K. Kubodera, Nucl. Phys. A **500**, 429 (1989).